A&A 404, 355–364 (2003)
DOI: 10.1051/0004-6361:20030482


Astronomy & Astrophysics

# The corona of V390 Aurigae (HD 33798)

P. Gondoin⋆

European Space Agency, ESTEC, Postbus 299, 2200 AG Noordwijk, The Netherlands

Received 3 December 2002 / Accepted 24 March 2003

**Abstract.** V390 Aurigae (HD 33798) is a rapidly rotating, lithium rich, late-type giant whose distinctive characteristics include a high X-ray luminosity observed by the *XMM–Newton* space observatory. Series of lines of highly ionized Fe and several Lyman lines of hydrogen-like ions and triplet lines of helium-like ions are visible in the reflection grating spectra, most notably from O and Ne. X-ray emission from plasma at high temperature ($T > 10^7$ K) indicates intense flaring activity on this star. Analysis results suggest a scenario where the corona of V390 Aurigae is dominated by large magnetic structures similar in size to interconnecting loops between solar active regions but significantly hotter. The interaction of these structures could explain the permanent flaring activity on large scales that is responsible for heating plasma to high temperatures. The intense activity on V390 Aurigae is related to its evolutionary position at the bottom of the red giant branch. It is anticipated that the rotation of the star will spin-down in the future, thus decreasing the efficiency of its $\alpha - \Omega$ dynamo with the suppressing of large scale magnetic structures in its corona.

**Key words.** stars: individual: V390 Aurigae – stars: activity – stars: coronae – stars: evolution – stars: late-type – X-ray: stars

## 1. Introduction

V390 Aurigae (HD 33798) is a chromospherically active late−type giant (see Table 1). Gurzadyan (1975) detected ultraviolet Mg II emission and Bidelman (1985) identified it as a Ca II emission star with moderate emission. A surface flux level $\log F(K) = 6.3$ of the Ca II K line was measured by Strassmeier et al. (1990). Spurr & Hoff (1987) determined a photometric period, assumed to be the rotation period of the star, of only 9.8 days which was later refined to 9.825 days by Hooten & Hall (1990). Fekel & Marshall (1991) found that the best fit to the spectrum of HD 33798 in the 6430 Å region is obtained with $\kappa$ Gem, a G8 III star. This spectral type corresponds to an effective temperature of 4970 K (Bell & Gustafsson 1989). V390 Aurigae is the primary of the visual binary ADS 3812 whose secondary is $0.358'' \pm 0.011''$ away and $\Delta m_V = 1.85 \pm 0.08$ fainter (ESA 1997). It was designated as V390 Aurigae by Kholopov et al. (1989) in the 69th name list of variable stars. Flare activity has been detected by Konstantinova-Antova et al. (2000). Some properties of V390 Aurigae are reminiscent of those of the RS CVn binaries. However, Fekel & Marshall (1991) found no periodic variation in an analysis of 40 radial velocity measurements and concluded that the star is single. These authors also noticed that its space motion is similar to that of FK Comae and that its rapid rotation ($v \sin i = 29 \pm 1$ km $^{-1}$) is quite unusual. Other characteristics of V390 Aurigae include an X-ray luminosity (Hünsch et al. 1998) exceptionally high for a red giant. We report on an analysis of X-ray spectra of V390 Aurigae registered during two observations performed in September 2000 and in March 2001 by the *XMM–Newton* observatory. The observations were conducted with the aim to improve our understanding of the magnetic activity on giants like V390 Aurigae by investigating the origin of its high X-ray luminosity and the structure of its X-ray corona.

⋆ e-mail: pgondoin@rssd.esa.int

**Table 1.** Top: $V$ magnitudes, parallaxes and absolute magnitudes of V390 Aurigae. Middle: spectral type, color indices and effective temperature. Bottom: estimated stellar parameters of V390 Aurigae.

| $V$ | par (mas) | $M_V$ |
|---|---|---|
| 6.91 | 8.947±1.35 | 1.68 |
| Sp. Type | $B-V$ | $T_{\rm eff}$ (K) |
| G8 III | 0.982 | 4970 |
| $R$ ($R_\odot$) | $v_{\rm eq}$ (km s$^{-1}$) | $M$ ($M_\odot$) |
| 6.7 | 35 | 1.8 |

This paper is organized as follows. Section 2 provides the stellar parameters of V390 Aurigae and compares its evolution status with those of nearby single field giants in light of *Hipparcos* parallaxes (ESA 1997). Section 3 describes the X-ray observations of V390 Aurigae and the data reduction procedures. Section 4 then presents the integrated flux measurements and their temporal behavior during the observations. Section 5 describes the spectral analysis of the EPIC and RGS data sets. Finally, a physical interpretation of the analysis results is proposed in Sect. 6. In this last section, the structure of V390 Aurigae corona and its possible evolution are discussed within the frame of stellar activity evolution across the Hertzsprung gap.

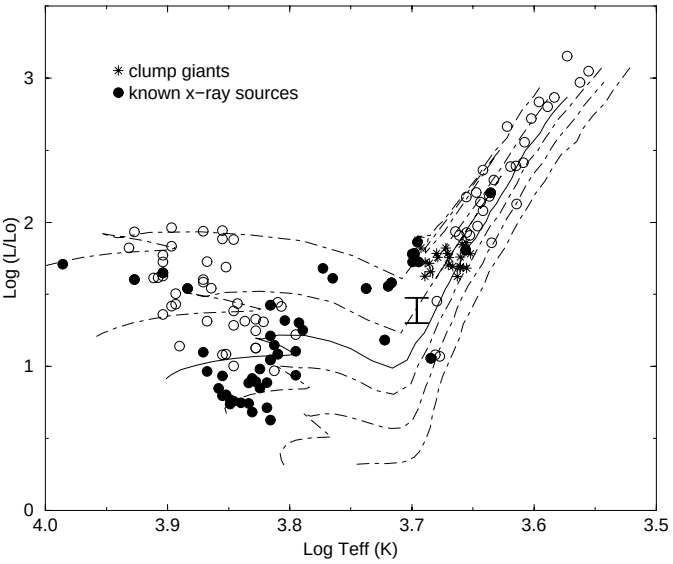


**Fig. 1.** H–R diagram of single giants (Gondoin 1999) compared with evolutionary tracks (Schaller et al. 1992) of 1 $M_\odot$ (lower dashed line), 1.25 $M_\odot$, 1.5 $M_\odot$, 1.7 $M_\odot$ (solid line), 2 $M_\odot$ and 2.5 $M_\odot$. Black circles mark giants known as X-ray sources. The H–R diagram location of V390 Aurigae is indicated by an error bar.

## 2. V390 Aurigae stellar parameters

Differential photometry observations reported by Hooten & Hall (1990) on V390 Aurigae show that its $V$ magnitude varies with a full amplitude of 0.380 and a period of 9.825 days. This period with $v \sin i = 29$ km s$^{-1}$ measured by Fekel & Marshall (1991) results in $R \sin i = (5.6 \pm 0.4)\, R_\odot$ (Drake et al. 2002). The *Hipparcos* parallaxes ($\pi = 8.94 \pm 1.35$ mas; ESA 1997) lead to an absolute magnitude $M_V = 1.68$, a stellar radius $R = 6.7\, R_\odot$ and an equatorial velocity $v_{\rm eq} = 35$ km s$^{-1}$. This rapid rotation is a striking peculiarity of V390 Aurigae in regard to its spectral type. One hypothesis to explain the rapid rotation and activity of the star is the existence of a tiny but as yet unseen companion, which dumps mass onto the visible component thus producing a significant angular momentum transfer. However, no radial velocity variation characteristic of orbital motion has been detected. The data of Fekel & Marshall (1991) have made this small companion hypothesis extremely unlikely, and the origin of V390 Aurigae is still a matter of debate.

Another possible scenario is that the star originates from an early type, rapidly rotating, single star as it evolves in the giant domain. Li abundance measurements (Fekel & Balachandran 1990) support this scenario in which the star has recently crossed the Hertzsprung gap and became a convective late-type giant. At a later evolutionary stage when the star ascends the red giant branch, the inward expansion of its convective envelope is expected to transport Li from the surface to the interior thus reducing its surface abundance by dilution. If V390 Aurigae were a clump giant in an even more advanced stage of evolution associated with the helium core burning phase, the fully formed convective envelope would have completely diluted the surface lithium remaining at the end of the main sequence lifetime. Figure 1 compares the H–R diagram positions of V390 Aurigae and single nearby giants (Gondoin 1999) with evolutionary tracks of stellar models with near solar metallicity (Schaller et al. 1992). V390 Aurigae occupies a particular region near the bottom of the red giant branch (RGB) close to the evolutionary tracks of a 2.0 $M_\odot$ star. This corroborates the hypothesis that V390 Aurigae could have normally evolved from an A-type main sequence star. An alternative hypothesis to explain the rapid star rotation is that V390 Aurigae results from merging of a close binary system such as a W Ursae Majoris system (Collier Cameron 1982). However, if that is so, the large lithium abundance needs to be explained since such an event would probably dilute the surface lithium.

## 3. Observations and data reduction

V390 Aurigae was observed twice by the *XMM–Newton* space observatory (Jansen et al. 2001), respectively in revolutions 135 on 2000 September 4 and 235 on 2001 March 15 (see Table 2). The satellite observatory uses three grazing incidence telescopes which provide an effective area higher than 4000 cm$^2$ at 2 keV and 1600 cm$^2$ at 8 keV (Gondoin et al. 2000). Three CCD EPIC cameras (Strüder et al. 2001; Turner et al. 2001) at the prime focus of the telescopes provide imaging in a 30 arcmin field of view and broadband spectroscopy with a resolving power of between 10 and 60 in the energy band 0.3 to 10 keV. Two identical RGS reflection grating spectrometers behind two of the three X-ray telescopes allow higher resolution ($E/\Delta E = 100$ to 500) measurements in the soft X-ray range (6 to 38 Å or 0.3 to 2.1 keV) with a maximum effective area of about 140 cm$^2$ at 15 Å (den Herder et al. 2001).

V390 Aurigae observations were conducted with the EPIC cameras operating in full frame mode (Ehle et al. 2001). RGS spectra were recorded simultaneously. "Thick" aluminium filters were used in front of the EPIC MOS cameras and "medium" thickness aluminum filters were used in front of EPIC p−n cameras to reject visible light. Processing of the raw event data set was performed using the "emchain", "epchain" and "rgsproc" pipeline tasks of the *XMM–Newton* Science Analysis System (SAS version 5.3.0). V390 Aurigae spectra were built from photons detected within windows of about 40″ diameter around the target bore-sight in the EPIC cameras. The background was estimated on the same CCD chips as the source, within windows of similar sizes which were offset from the source position in an empty field region. About 30% of revolution 135 exposure was discarded from the EPIC spectral analysis. The rejected events were those occurring during time intervals with a high level of magnetospheric background protons. Due to a lower level of background, the entire exposure of revolution 232 could be analyzed. The Pulse-Invariant (PI) spectra were rebinned such that each resulting MOS channel had at least 20 counts per bin and each p−n channel had at least 40 counts per bin. $\chi^2$ minimization was used for spectral fitting. All fits were performed using the XSPEC package (Arnaud & Dorman 2001). The EPIC and RGS response matrices were generated by the SAS task "rmfgen" and "rgsrmfgen" respectively. EPIC p−n, MOS 1 and MOS 2 spectra were fitted together in the 0.3 to 4 keV energy range in revolution 135 and in the 0.3 to 8 keV energy range

**Table 2.** V390 Aurigae observation log during *XMM–Newton* revolution 135 and 232.

| Rev. | Experiment | Filter | Mode | Start Exp. (UT) | Exp. Duration |
|---|---|---|---|---|---|
| | MOS1 | Thick | Prime Full | 2000-09-04@04:32:27 | 19 687 s |
| | MOS2 | Thick | Prime Full | 2000-09-04@04:32:27 | 19 734 s |
| 135 | p−n | Medium | Prime Full | 2000-09-04@05:13:52 | 18 008 s |
| | RGS1 | | Spec + Q | 2000-09-04@04:24:01 | 16 525 s |
| | RGS2 | | Spec + Q | 2000-09-04@04:24:01 | 25 354 s |
| | MOS1 | Thick | Prime Full | 2001-03-15@18:38:01 | 21 894 s |
| | MOS2 | Thick | Prime Full | 2001-03-15@18:38:01 | 21 894 s |
| 232 | p−n | Medium | Prime Full | 2001-03-15@18:38:44 | 18 725 s |
| | RGS1 | | Spec + Q | 2001-03-15@18:39:43 | 22 454 s |
| | RGS2 | | Spec + Q | 2001-03-15@18:39:43 | 22 454 s |

in revolution 232. The upper cut-off of the spectral band was imposed by the decreasing count rate at high energies. The RGS spectra were analyzed separately due to their higher spectral resolution in the 0.3−2.1 keV energy range.

## 4. Integrated flux and temporal behavior

Figure 2 shows the light curves of V390 Aurigae obtained during revolution 135 and 232 with the p−n camera after subtraction of background events. The count rate was about 50% higher in revolution 232 with an average count rate of $1.33 \pm 0.09$ s$^{-1}$ compared with a count rate of $0.89 \pm 0.07$ s$^{-1}$ in revolution 135. The 2–10 keV over 0.3–2 keV count rate ratios were respectively $37 \pm 5$ and $43 \pm 27$ during revolutions 135 and 232 respectively, indicating that the spectrum of V390 Aurigae was soft during both observations. The count rate in the low energy band decreased steadily by ≈3% within 17 ksec and by 4.5% within 19 ksec during revolution 135 and 232, respectively.

The spectral analysis of each observation were conducted separately. Spectral fitting of the EPIC data (see Sect. 5) during these two periods yields flux measurements in the 0.3–2 keV and >2 keV bands. These measurements were converted into X-ray luminosities $L_{0.3-2\ \mathrm{keV}}$ and $L_{>2\ \mathrm{keV}}$ using the *Hipparcos* parallax ($\pi = 8.94$ mas; ESA 1997). The luminosities are given in Table 3 which also provides the hardness ratio *hr* of the X-ray emission defined as $hr = (L_{>2\ \mathrm{keV}} - L_{0.3-2\ \mathrm{keV}})/(L_{>2\ \mathrm{keV}} + L_{0.3-2\mathrm{keV}})$. Table 3 confirms that the X-ray spectrum of V390 Aurigae is soft. Compared with revolution 135, the X-ray luminosity of V390 Aurigae during revolution 232 was 35% higher in the 0.3–2 keV band and a factor of 2 larger in the high energy band.

## 5. Spectral analysis

### 5.1. Analysis of EPIC data

The two EPIC data sets (see Fig. 3) were fitted separately with the MEKAL optically thin plasma emission model (Mewe et al. 1985). The spectral fitting was performed in the 0.3–4 keV and 0.3–8 keV spectral bands for revolutions 135 and 232, respectively since revolution 135 data does not contain any significant signal above 4 keV. The interstellar hydrogen column density was left free to vary. A consistent value $N_{\mathrm{H}} = 3.2 \times 10^{20}$ cm$^{-2}$ was derived from the analysis of the two data sets. It is significantly lower than the total galactic H I column density $N_{\mathrm{H}} = 4.61 \times 10^{21}$ cm$^{-2}$ (Dickey & Lockman 1990) in the direction of V390 Aurigae. A smaller column density ($N_{\mathrm{H}} = 1.5 \times 10^{18}$ cm$^{-2}$) is found on the line of sight to G191-B2B, which is located only a few degrees away from V390 Aurigae at a distance of 68.8 pc (Lemoine et al. 2002). Such a difference on the hydrogen column density may be related to calibration uncertainties of the EPIC camera at low energies or missing lines in the plasma spectroscopy code. If so, they would not impact the analysis results presented hereafter.

No single temperature plasma model that assumes either solar photospheric (Anders & Grevesse 1989) or non solar abundances can fit the data, as unacceptably large values of $\chi^2$ were obtained. The MEKAL plasma models with two components at different temperatures prove adequate for the two data sets (see Table 4). MEKAL plasma models with three components at different temperatures only gives a marginal improvement to the fit of revolution 232 data set and the emission measure and temperature of the additional plasma component are poorly constrained.

In the two component model, the temperature of the cool plasma is the same (≈0.6 keV) for revolution 135 and 232. Hot ($kT > 1$ keV) plasma on V390 Aurigae is the main source of X-ray emission in the hard X-ray band. It contributes more than 79% of the X-ray luminosity above 2 keV in revolution 135 and more than 90% in revolution 232. Table 4 shows that the increase of V390 Aurigae X-ray luminosity between revolution 135 and 232 both in the soft and in the hard energy range are almost entirely related to an increase in emission measure of this hot ($kT > 1$ keV) plasma. Furthermore, its temperature is higher ($kT \approx 1.2$ keV) during revolution 232 when the star is more X-ray luminous. The average element abundance in V390 Aurigae corona is found to be lower than the

**Table 3.** X-ray luminosities (corrected for interstellar absorption) of V390 Aurigae in the 0.3−2 keV and 2−10 keV bands. The percentage contribution in luminosity of hot plasmas ($kT > 1$ keV) is indicated between brackets.

| Obs. | $L_{0.3-2\ \mathrm{keV}}$ ($10^{30}$ erg s$^{-1}$) | $L_{2-10\ \mathrm{keV}}$ ($10^{30}$ erg s$^{-1}$) | *hr* |
|---|---|---|---|
| Rev. 135 | 3.90 | 0.30 | −0.86 |
| | (41%) | (79%) | |
| Rev. 232 | 5.27 | 0.61 | −0.79 |
| | (55%) | (90%) | |

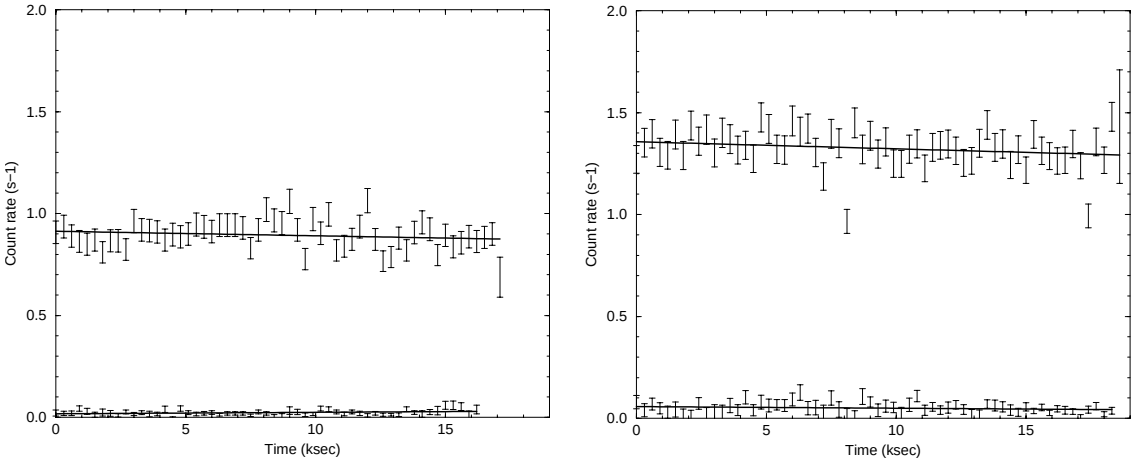


**Fig. 2.** Light curves of V390 Aurigae during revolutions 135 (left) and 232 (right) obtained with the EPIC p−n camera. In each graph, the upper curve is the count rate within the 0.3 to 2 keV band and the lower curve is the count rate within the 2 to 10 keV band. The events are binned in 300 s time intervals and the background has been subtracted.

solar photospheric value (see Table 4). The apparently higher metallicity of the cool component during revolution 232 is not significant at the 90% confidence level. The derived abundances are relatively similar for the two plasma components and no significant abundance variations are detected between the two revolutions.

### 5.2. Analysis of RGS data

Figure 4 shows the RGS spectra averaged over revolution 135 and over revolution 232. Each spectrum is the sum of the two spectra simultaneously obtained with the RGS1 and RGS2 reflection grating spectrometers on board *XMM–Newton*. For line identification, we required only that the wavelength coincidence be comparable to the spectral resolution of the RGS spectrometers, namely 0.04 Å over the 5 to 35 Å wavelength range. In the X-ray domain, many candidate lines may exist within this acceptable wavelength coincidence range. Hence, we only looked for resonance transitions of abundant elements and predicted line intensities using spectra of the Sun (Doschek & Cowan 1984) and of Capella (Brinkman et al. 2000). Series of lines of highly ionized Fe and several Lyman lines of hydrogen-like ions and triplet lines of helium-like ions are visible in RGS spectra, most notably from O and Ne. The strongest lines are listed in Table 5. Their temperatures of maximum formation range between 3 and $7\times10^6$ K indicating that the corresponding ions are mainly associated with the cool plasma component inferred from EPIC data. Line fluxes were measured using XSPEC by fitting the RGS spectra with Gaussian profiles, which represent the observed line profiles very well. Line fluxes corrected for interstellar absorption on the line of sight to V390 Aurigae are given in Table 5. Flux measurements of the Ne X (12.13 Å) and O VIII (16.01 Å) lines are affected by blends. Table 5 shows that difference in line intensities between revolutions 135 and 232 are not significant at the 90% confidence level. The low signal to noise ratio of RGS spectra prevents detection and flux estimate of emission lines outside the 10–20 Å spectral range.

We fitted the low energy RGS spectra obtained in revolution 135 and 235 by a VMEKAL model with two component at different temperatures. The VMEKAL model generates a spectrum of hot diffuse gas with line emission from several elements based on the calculation of Mewe et al. (1985) with Fe L calculations by Liedahl (1995). Hence, two electron temperatures and electron densities are assumed for the entire ensemble of element charge states and in particular for iron, oxygen and neon which produce the most prominent lines. This assumption turns out to be fairly adequate within the observational uncertainties of the present spectrum. The fit was performed in the spectral range from 10 Å to 20 Å where the efficiency of the RGS spectrometers is the highest. The model temperatures and abundances of the cool and hot plasma components were frozen to the values derived from EPIC data (see Table 4) since their determination requires an accurate measurement of the X-ray continuum which cannot be reliably measured from the RGS spectra (see Fig. 4) due to a moderate spectral resolution and signal to noise ratio. The abundances of the O and Ne elements which give prominent lines in the considered spectral range were then allowed to vary. No significant abundance variation of O and Ne with respect to other elements were detected for the cool plasma component. Fitting results with variable O and Ne abundances for the hot component are given in Table 6. The fit supports the two-component plasma model for the interpretation of the EPIC and RGS data. It suggests that the emission measure distribution of the plasma in the corona of V390 Aurigae exhibits two peaks at distinct temperatures in agreement with EPIC data analysis results. The coronal emission measure distribution has been found to be double peaked for many stars (Schrijver et al. 1995; Mewe et al. 1996; Güdel et al. 1997a, 1997b). However, as spatially unresolved observations gain in spectral resolution and signal to noise ratio, the amount of detail in the spectra of stellar coronae which must be reproduced increases reflecting the true complexity of the sources plasma. Recent analysis of *XMM–Newton* and *Chandra* X-ray spectra find that a continuous emission measure distribution fits the spectra better and is more realistic

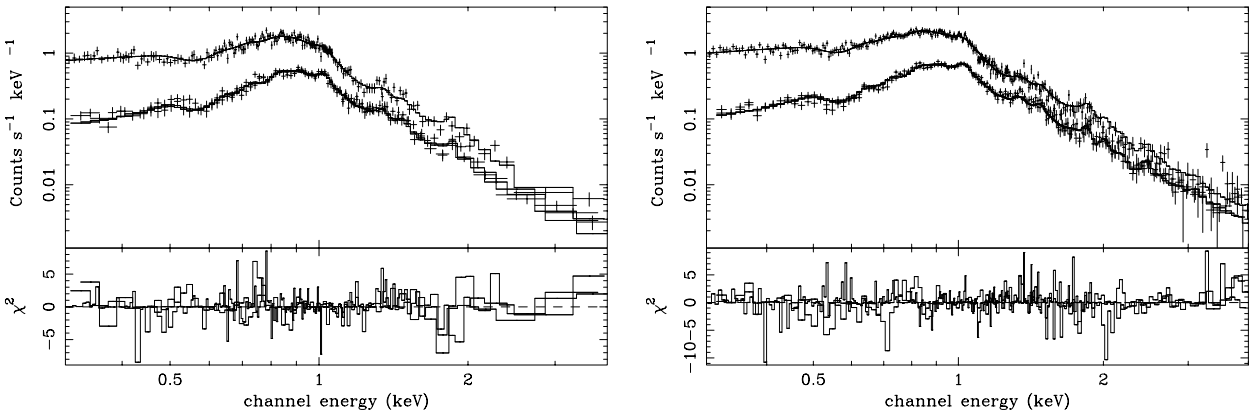


**Fig. 3.** Best fit model to revolution 135 (left) and 232 (right) spectra. The EPIC data (crosses) and spectral fit (solid line) are shown in the upper panel. The $\chi^2$ contributions are given in the lower panel of each graph.

**Table 4.** Best fit parameters to EPIC data using a two component MEKAL model (Mewe et al. 1985) with variable abundance and a variable hydrogen column density.

| Obs. | Cool | plasma | component | Hot | plasma | component | |
|---|---|---|---|---|---|---|---|
| | $Z$ | $kT$ (keV) | $EM$ ($10^{52}$ cm$^{-3}$) | $Z$ | $kT$ (keV) | $EM$ ($10^{52}$ cm$^{-3}$) | $\chi^2$ |
| Rev. 135 | 0.29 ± 0.09 | 0.62 ± 0.01 | 22 ± 14 | 0.23 ± 0.05 | 1.09 ± 0.05 | 20 ± 7 | 407/371 d.o.f. = 1.10 |
| Rev. 232 | 0.46 ± 0.19 | 0.63 ± 0.01 | 16 ± 13 | 0.22 ± 0.03 | 1.20 ± 0.03 | 39 ± 6 | 681/574 d.o.f. = 1.19 |

**Table 5.** Measured positions and fluxes of the strongest lines in the RGS spectra of V390 Aurigae obtained during revolutions 135 and 232. The columns give the predicted line positions, the measured line positions during revolution 135, the measured line positions during revolution 232, the ion and line identifications, the temperatures of maximum line formation, the line fluxes measured during revolution 135 and the line fluxes measured during revolution 232.

| $\lambda_{\rm pred}$ (Å) | $\lambda_{\rm rev135}$ (Å) | $\lambda_{\rm rev232}$ (Å) | Ion | line ID | log ($T_{\rm m}$) log (K) | $F_{\rm rev135}$ ($10^{-6}$ cm$^{-2}$ s$^{-1}$) | $F_{\rm rev232}$ ($10^{-6}$ cm$^{-2}$ s$^{-1}$) |
|---|---|---|---|---|---|---|---|
| 12.13 | 12.15 | 12.12 | Ne X | H1AB | 6.80 | 68 ± 14 | 64 ± 18 |
| 12.12 | | | Fe XVII | 4C | 6.75 | | |
| 13.45 | 13.45 | 13.54 | Ne IX | He4w | 6.60 | 57 ± 12 | 65 ± 18 |
| 14.26 | 14.25 | 14.23 | Fe XVIII | F1-52,53 | 6.80 | 46 ± 11 | 68 ± 13 |
| 15.01 | 15.00 | 15.01 | Fe XVII | 3C | 6.70 | 77 ± 14 | 66 ± 13 |
| 16.01 | 16.00 | 16.00 | O VIII | H2 | 6.60 | 41 ± 10 | 44 ± 11 |
| 16.07 | | | Fe XVIII | F3 | 6.80 | | |
| 16.79 | 16.67 | 16.77 | Fe XVII | 3F | 6.70 | 30 ± 10 | 44 ± 12 |
| 17.05 | 17.07 | 17.08 | Fe XVII | 3G | 6.70 | 69 ± 15 | 110 ± 21 |
| 17.10 | | | Fe XVII | M2 | 6.70 | | |
| 18.97 | 18.95 | 18.95 | O VIII | H1AB | 6.50 | 79 ± 17 | 65 ± 14 |

physically (Audard et al. 2001a,b; Güdel et al. 2001b; Mewe et al. 2001). We tried to fit the RGS spectra of V390 Aurigae first using a plasma model with a simple continuous emission measure distribution which is a power law function of the temperature of the type $EM(T) \approx (T/T_{\rm max})^{\alpha}$, where the maximum temperature of the plasma $T_{\rm max}$ and the slope of the emission $\alpha$ are treated as free parameters (Schmitt et al. 1990). The abundance of oxygen and neon were allowed to vary independently from the abundances of the other elements. An acceptable fit to the RGS spectra ($\chi^2 = 1.16$ for 200 degree of freedom) is obtained only for revolution 135. The steep slope ($\alpha = 3.4 \pm 1.1$) indicates that most of the emission is concentrated at the maximum temperature of the model ($kT_{\rm max} = 0.78 \pm 0.05$ keV). This temperature is intermediate between the cool and hot plasma temperatures of the two component MEKAL model (see Table 4). The abundance of oxygen equals that of other elements ($0.14 \pm 0.04$) but is lower than the abundance derived from the EPIC data (see Table 4). The fitting with a power law emission measure distribution also indicates a neon abundance enhancement (by about a factor of 2) relative to oxygen. We also tried to fit the RGS spectra of V390 Aurigae with a more complex plasma model using a continuous emission measure distribution parameterized by the exponential of a sum of terms of a 6th order Chebyshev polynomial in the log ($EM$) – log ($T$)

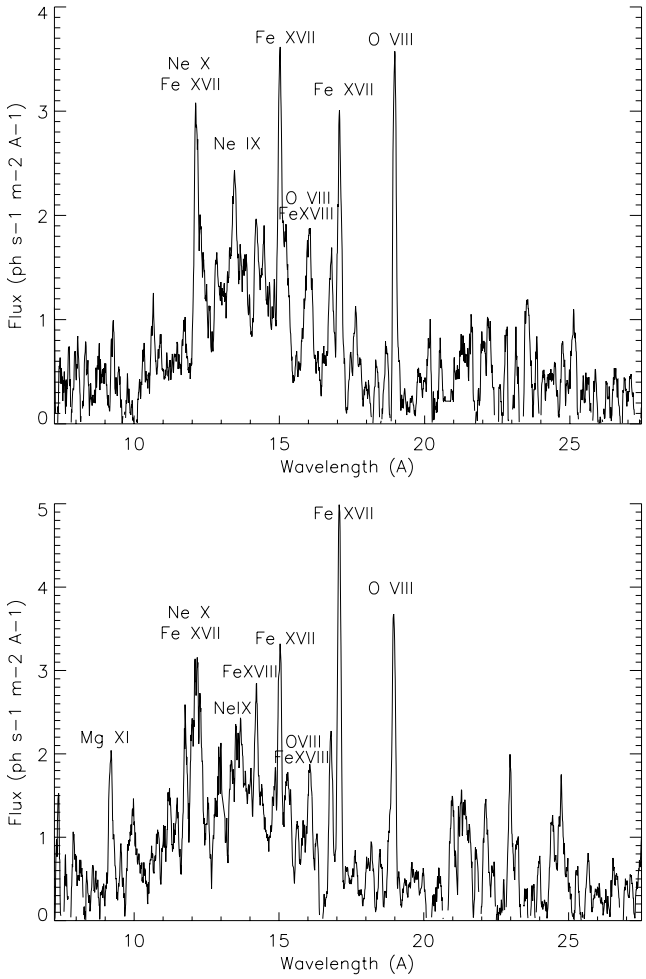


**Fig. 4.** Averaged first order spectra of RGS 1 and 2 obtained during revolution 135 (top) and revolution 232 (bottom).

plane (Lemen et al. 1989). The polynomial coefficients could not be constrained by the data due to the moderate signal to noise ratio.

The best fit models with either discrete or continuous emission measure distribution indicate that the oxygen abundance is similar to the average abundance of the other elements. Using the Anders & Grevesse (1989) table, this abundance (see Table 6) translates into $\log(\epsilon(\mathrm{O})) = 8.35 \pm 0.4$, a value comparable with a recent measurement of the oxygen abundance in the solar photosphere ($\log(\epsilon(\mathrm{O})) = 8.69 \pm 0.05$; Allende Prieto et al. 2001) which is smaller than older values usually cited. The measurement of abundances relative to hydrogen requires an accurate determination of the X-ray continuum which is modelled from the flux left over when all of the known emission lines in the VMEKAL model are included. Since no plasma spectroscopy code includes all of the emission lines, the missing weak emission lines could be misinterpreted as continuum flux (Schmitt et al. 1996), thereby raising the hydrogen abundance derived from the free-free continuum and lowering all of the metal abundances relative to hydrogen. This systematic error in the metal abundances relative to hydrogen is however negligible with respect to the abundance uncertainties stated in Table 6 and the fitting results suggest that neon

**Table 6.** Best fit parameters to RGS spectra in the 0.6–1.3 keV range recorded in revolutions 135 and 232 using a two component VMEKAL model. The temperature and metallicity of each component were frozen to the value derived from the analysis of EPIC data (see Table 4). The oxygen and neon abundances of the high temperature component were left free to vary.

| Model | Parameter | Rev. 135 | Rev. 232 |
|---|---|---|---|
| WABS | $n_{\mathrm{H}}$ ($\mathrm{cm}^{-2}$) | $3.19 \times 10^{20}$ | $3.19 \times 10^{20}$ |
| VMEKAL | $kT$ (keV) | 0.62 | 0.63 |
| (low T) | Other abundances | 0.23 | 0.46 |
| | $kT$ (keV) | 1.09 | 1.20 |
| VMEKAL | O | 0.5 ± 0.2 | 0.2 ± 0.1 |
| (high T) | Ne | 1.5 ± 0.7 | 0.5 ± 0.3 |
| | Other abundances | 0.29 | 0.22 |
| | $\chi^2$ | 1.14 (230/202) | 1.18 (235/199 d.o.f.) |

abundance of the hot plasma component is significantly higher than the oxygen abundance. The Ne/O ratio found for V390 Aurigae seems higher than in the solar photosphere. Such a Ne abundance enhancement is reminiscent of a similar anomaly observed in a subset of solar flares (Murphy et al. 1991; Schmelz 1993). Large Ne abundance enhancements are a common feature of active stellar coronae (Güdel et al. 2001; Huenmoerder et al. 2001) and an inverse FIP effect is observed in very active coronae (Brinkman et al. 2001; Drake et al. 2001) where the abundances (relative to oxygen) increase with increasing first ionization potential (FIP).

The emitting volume of the different plasma components could be constrained if their electron densities were known. These can be measured using density sensitive spectral lines originating from metastable levels, such as the forbidden (f) $2^3\mathrm{S}-1^1\mathrm{S}$ line in helium like ions (Ness et al. 2001, 2002). This line and the associated resonance (r) $2^1\mathrm{P}-1^1\mathrm{S}$ and inter-combination (i) $2^3\mathrm{P}-1^1\mathrm{S}$ lines make up the so-called helium like triplet lines (Gabriel & Jordan 1969; Pradhan 1982). The intensity ratio (i+f)/r varies with electron temperature and the ratio i/f varies with electron density due to the collisional coupling between the metastable $2^3\mathrm{S}$ upper level of the forbidden line and the $2^3\mathrm{P}$ upper level of the inter-combination line. The RGS wavelength band contains the triplet lines of the helium-like ions O VII, Ne IX, Mg XI and Si XIII. However, the Si, Mg and O triplets are not detected in the RGS spectra of V390 Aurigae and the Ne IX triplet is too heavily blended with iron and nickel lines for density analysis.

## 6. Discussion

### 6.1. Structure of V390 Aurigae corona

The spectral fitting of the EPIC and RGS spectra of V390 Aurigae with a two component model suggests a corona configuration with little contribution from quiet regions similar to the Sun. On the contrary the 0.6 keV temperature of the "cool" plasma component is reminiscent of solar type active regions, while the hot ($kT > 1$ keV) component may be caused by disruptions of magnetic fields associated to a

permanent flaring activity. The review of coronal activity by Vaiana & Rosner (1978) pointed out that the Sun, if completely covered with active regions, would have an X-ray luminosity of $2 \times 10^{29}$ ergs s$^{-1}$. When scaled to the surface of V390 Aurigae ($R \approx 6.7\ R_\odot$; see Table 1), an X-ray luminosity of $9 \times 10^{30}$ erg s$^{-1}$ is obtained. This value is comparable with the observed X-ray luminosity of V390 Aurigae (4 to $7 \times 10^{30}$ erg s$^{-1}$) derived using *Hipparcos* parallax and higher than the X-ray luminosity contribution ($\approx 2.4 \times 10^{30}$ erg s$^{-1}$) of its "cool" ($kT \approx 0.6$ keV) plasma component. The X-ray luminosity of the "cool" component could be explained if 25–30% of the surface of V390 Aurigae is covered with bright solar like active regions. Assuming that these active regions can be described by a simple static loop system consisting of similar loops of constant pressure $p$ (dyn cm$^{-2}$), temperature $T$ (K) and cross section $A$ (cm$^2$), the emission measure $EM$ (cm$^{-3}$) of the "cool" plasma can be expressed as:

$$EM = GF \times (4\pi R^2) \times (p/2kT)^2 \times L \quad (1)$$

where $R$ is the stellar radius, $F$ is the filling factor and $L$ the loop half-length. $G$ is a geometry factor which includes effect of partial occultation of the corona by the star itself (i.e. $G$ varies from 0.5 to 1 for $L \ll R$ to $L \gg R$). Using the RTV scaling law $T = 1400(pL)^{1/3}$ (Rosner et al. 1978) and $G = 0.7$, a characteristic loop length scale is obtained (Mewe et al. 1982):

$$L_{10} = 7.4F \times T_7^4 \times EM_{52}^{-1} \times (R/R_\odot)^2 \quad (2)$$

where $L_{10}$ is the loop half length in units of $10^{10}$ cm, $T_7$ is the coronal temperature in unit of $10^7$ K, and $\mathrm{EM}_{52}$ is the emission measure in units of $10^{52}$ cm$^{-3}$. The standard static steady state model of Rossner et al. (1978) makes simplifying assumptions, such as a constant pressure along the loop, and a uniform heating function. Solar *TRACE* data indicate that these assumptions are often not valid. Solar observations confirm the RTV scaling law essentially for hot ($T_\mathrm{e} > 2$ MK) and short ($L < 10^{10}$ cm) loop, while it has been found to be invalid for cooler ($T_\mathrm{e} < 2$ MK) and larger ($L > 10^{10}$ cm) loops (Aschwanden et al. 2000). Inserting the observed temperature and emission measure of the cool plasma component of V390 Aurigae (see Table 4) and $R = 6.7\ R_\odot$ (see Table 1) in Eq. (2), we find $L \approx 4.7 \times F \times 10^{10}$ cm$^{-3}$. Assuming a 25–30% filling factor, we derive the corresponding value of loop base pressure and half-length (see Table 7). Since it turns out that the loop length are much smaller than the pressure scale height $H$, the assumption of constant pressure in the loops is justified. Characteristic loop size and temperature on V390 Aurigae are respectively $1.3 \times 10^{10}$ cm and $7.2 \times 10^6$ K. Solar corona observations by comparison show bright hot loops within active regions which reach maximum temperatures and electron densities above the neutral line of typically $(3\text{–}4) \times 10^6$ K and $10^{10}$ cm$^{-3}$ (Vaiana et al. 1973). In addition to these hot loops, on-disk images of the Sun show that neighboring active regions are often connected into complexes of activity by large loop-like structures (van Speybroek et al. 1970). Such interconnecting loops can be $>10^{10}$ cm long, i.e. as long as the loop length estimate on V390 Aurigae. However, they tend to be cooler than loops within solar active regions and therefore cooler than coronal loops on V390 Aurigae.

**Table 7.** Physical parameters of V390 Aurigae coronal loops.

| $T$ (K) | $EM$ (cm$^{-3}$) | $H$ (cm) | $L$ (cm) | $n$ (cm$^{-3}$) |
|---|---|---|---|---|
| $7.2 \times 10^6$ | $19 \times 10^{52}$ | $93 \times 10^{10}$ | $1.3 \times 10^{10}$ | $11 \times 10^9$ |

If in V390 Aurigae, the cool plasma components is produced by solar like active regions covering a large fraction of the star's surface, it is easy to imagine that such a dense population of active regions coexists with constant interaction and disruption of their magnetic fields which might be expected to lead to continuous flaring. This could explain the permanent emission measure of hot plasma above 1 keV. High temperature plasmas constitute flare indicators which have been detected from the Sun and from non-solar coronae (van den Oord & Mewe 1989; Tsuru et al. 1989). The solar flare plasma shows a bimodal temperature distribution with plasma at two different temperatures 0.4–0.7 keV and 1.4–2.2 keV where the hot component is present only during the flares (Antonucci & Dodero 1995). The two components probably have a common origin in the flaring region on the Sun, since the component at 0.4–0.7 keV cools to active region temperatures of 0.2–0.3 keV during the flare decay (Antonucci & Dodero 1995). The temperatures of these components are close to the temperatures found in the X-ray emission from V390 Aurigae. There is also evidence that the emission measure distribution of very active stellar coronae, obtained from spectrally resolved XUV observations, is double-peaked with a peak often found above $10^7$ K (Griffiths & Jordan 1998). Recently, Sanz-Forcada et al. (2002) noticed that emission measure distribution are remarkably similar among a sample of RSCVn's binaries and single active stars including the low-rotation giant $\beta$ Cet, showing a narrow enhancement or bump around $\log T_\mathrm{e} \approx 6.9$. This aspect is debated but it has been suggested that this hot component may be due to a continuous flaring activity (Güdel 1997; Drake et al. 2000). The surface of active stars is covered by active regions, and flares would be so frequent that their light curves overlap, cancelling out any variability due to single events. Reale et al. (2001) showed that a double-peaked emission measure distribution is obtained if one combines the $EM(T)$ of the whole solar corona with the envelope of the $EM(T)$ profiles during solar flares. This seems to suggest that uninterrupted sequence of overlapping proper flares, whichever their evolution, could produce a double peak emission measure distribution in the coronae of active stars. This could explain the presence of hot coronal material even in the absence of obvious flares, which does not mean that there are no small scale flares not well identified in the light curve of XUV data with moderate signal to noise ratio. The flatness of the V390 Aurigae's light curve (see Fig. 2) could be explained by assuming that the heating of its corona results from a large number of small flares. Indeed, recent studies of the flare frequency in magnetically active stars as a function of the flare energy indicate power-law distributions that may be sufficient to explain all coronal radiative losses (Audard et al. 2000; Kashyap et al. 2002;

Güdel et al. 2003). One would however expect to see a few large flares that are not seen in V390 Aurigae data. Their absence might result from high energy cutoffs in the flare distribution (Kucera et al. 1997) related to the maximum energy that can be liberated in active regions on V390 Aurigae, constrained by their volume and the maximum magnetic field available in the photosphere. In a coordinated observing campaign on the short-period RS CVn binary $\sigma^2$CrB, Osten et al. (2003) detected multiple flares with the *Extreme Ultraviolet Explorer*, five occurring within three days. Remarkably, only one flare was detected at the end of the simultaneous but shorter one day *Chandra* observation with the notable absence of variation in the light curve during quiescence. This indicates that the short duration of the *XMM–Newton* observations of V390 Aurigae precludes further judgment on the flare frequency distribution and on the continuous flaring hypothesis.

Within the above interpretation, the higher emission measure and luminosity contribution of the hot plasma component in revolution 232 would be related to a more intense flaring activity of V390 Aurigae during March 2001. On the other hand, the steady flux decrease during revolution 135 and 232 could be interpreted as the gradual disappearance of active regions at the limb of the star. Hence, active regions might not be homogeneously distributed on the surface of the star. It is therefore difficult with the presented data to distinguish between a long-term variability of the flaring activity and a rotational modulation by long lived active regions. Furthermore, the above interpretation does not take into account a possible contribution to the X-ray luminosity of the secondary star in the ADS 3812 binary. Based on optical data, Konstantinova-Antova et al. (2000) believe that flare events in this binary system more likely happen on the primary star (V390 Aurigae) but, since the two companions are separated by only 0.358 arcsec, XMM–Newton cannot confirm that V390 Aurigae is the main X-ray source.

### 6.2. Evolution of V390 Aurigae corona

Possible hypotheses regarding V390 Aurigae origin (see Sect. 2) include evolution from either a single, rapidly rotating progenitor or from the merging of a close binary system. Leonard & Livio (1995) proposed that the product of mergers would gain a large amount of thermal energy in the collision. Under this assumption, such stars could be largely or fully mixed owing to convection despite the fact that the collision itself does not result in a significant amount of mixing (Sills et al. 1997). Although difficult to probe, this merger scenario could be expected to produce abundance anomalies in the atmosphere of the merger, which would persist as it becomes a cool giant (Schmitt & Ness 2002). Our X-ray measurements show that the average element abundance in V390 Aurigae corona is lower than the solar photospheric value. No abundance anomaly is found besides the neon abundance enhancement that can be attributed to flares. The single progenitor hypothesis remains a likely scenario providing that it accounts for the rapid rotation of the star.

The photometric period of V390 Aurigae is 9.825 days (Fekel & Marshall 1991), and a recent estimate of its

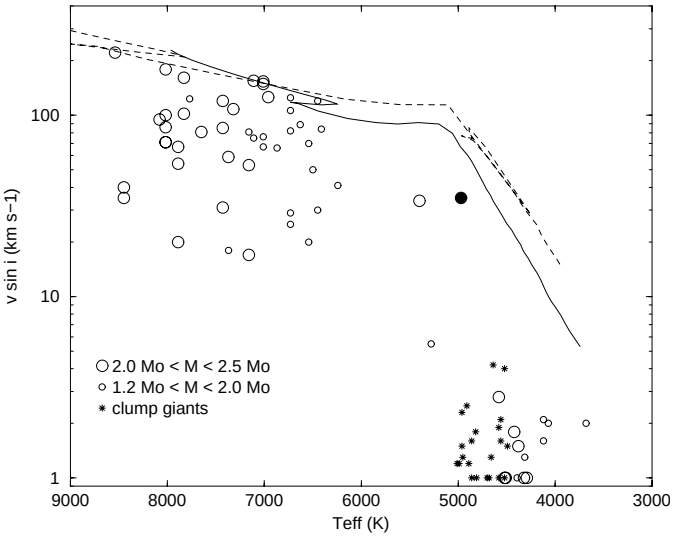


**Fig. 5.** Equatorial rotational velocity of V390 Aurigae (filled circle) compared with $v \sin i$ values of single field giants (Gondoin 1999). The solid line and the dashed line describe the equatorial velocity evolution of 1.7 $M_\odot$ and 2.5 $M_\odot$ stars respectively assuming angular momentum conservation and $v \sin i$ = 150 km s$^{-1}$ at $T_{\rm eff}$ = 7000 K.

equatorial velocity is 35 km s$^{-1}$ (see Table 1). We compared this value with $v \sin i$ values of A–F giants extracted from the Bright Star Catalogue and with $v \sin i$ measurements of G–K giants obtained with CORAVEL by de Medeiros & Major (1995). The CORAVEL measurements are precise to about 1 km s$^{-1}$. All projected equatorial velocity measurements are plotted in Fig. 5 as a function of $T_{\rm eff}$ for different mass ranges. A–F giants ($T_{\rm eff}$ > 6000 K) have high rotational velocities, often greater than 100 km s$^{-1}$. K giants, on the contrary, have low $v \sin i$ values of 1 or 2 km s$^{-1}$ for $T_{\rm eff}$ < 4700 K. As noticed by Simon & Drake (1989), stellar rotation strongly declines during the rapid evolution of G giants across the Hertzsprung gap. These authors also suggested, along with Gray (1989), that magneto-hydrodynamic braking due to stellar winds could explain this phenomenon. Rutten & Pylyser (1988) argued that during the entire evolution of a 3 $M_\odot$ star the timescale for magnetic braking is larger than the evolutionary time scale. Endal & Sofia (1979) and Gray & Endal (1982) pointed out that the expansion of the stars on the red giant branch together with the rearrangement of angular momentum due to the increasing depth of the convection zones may well explain the decrease of $v \sin i$ for cool giants. Gondoin et al. (2002) calculated the equatorial velocity evolution of 1.7 $M_\odot$ and 2.5 $M_\odot$ giants using Schaller et al. (1992) evolutionary models and assuming angular momentum conservation and $v \sin i$ = 150 km s$^{-1}$ at $T_{\rm eff}$ = 7000 K on the evolutionary tracks out of the main sequence. Comparisons of $v \sin i$ measurements with the theoretical model (see Fig. 5) confirm that angular momentum conservation alone cannot explain the rotational velocities of K giants. However, Fig. 5 suggests that V390 Aurigae, which is located near the bottom of the RGB, just starts experiencing rotational braking. The star developed an outer convective zone as it was evolving out of the main sequence across the mid-F spectral type. During its subsequent evolution, most of the angular

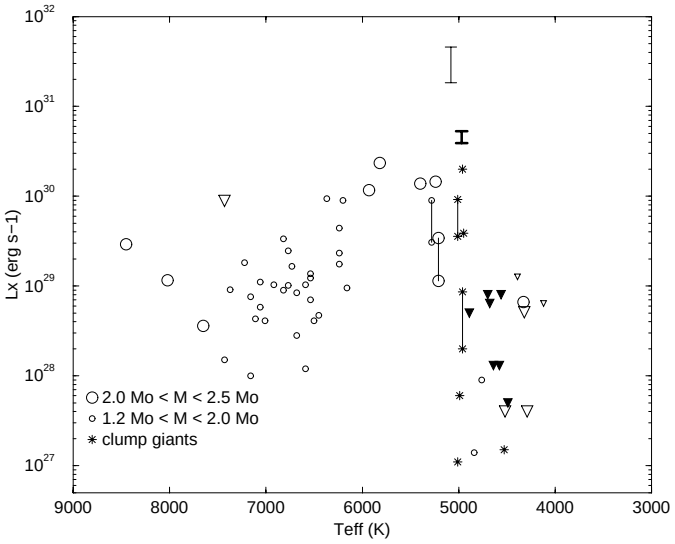


**Fig. 6.** The error bars in the upper part of the graph indicate the *XMM–Newton* luminosity range of FK Comae and of V390 Aurigae (bold bar) in the 0.3 to 2 keV band compared with ROSAT PSPC measurements of single field giants (Hünsch et al. 1998). Upper limits of X-ray luminosities measured with the Einstein observatory (Maggio et al. 1990) are indicated by small triangles, large triangles and filled triangles for low-mass ($1.2\ M_\odot < M < 2.0\ M_\odot$), intermediate-mass ($2.0\ M_\odot < M < 2.5\ M_\odot$) and clump giants respectively.

momentum would have been conserved within this convective envelope. A single progenitor hypothesis could then explain its rapid rotation.

Within this hypothesis, the outer convection zone of V390 Aurigae would have deepened since its formation, thus increasing the convective turnover time scale (Gilliland 1985). Since V390 Aurigae only experienced a small spin-down (see Fig. 5) and maintained a high rotation rate, the Rossby number (Durney & Latour 1978) decreased and dynamo activity increased as the star evolved towards the bottom of the RGB. During this period, the deepening convective envelope likely suffered shear stresses, which could have resulted in radial velocity gradients. The necessary conditions were then present to switch on an $\alpha$-$\Omega$ dynamo with an increasing efficiency as the star evolved towards the bottom of the RGB. Our spectral analysis of the X-ray data suggests that the large fluid kinetic helicity induced by the rapid rotation currently generates coronal magnetic fields with characteristic scale of $10^{10}$ cm, i.e. comparable with large interconnecting solar loops. The strong dynamo productive of large magnetic flux induces a large density of active regions covering up to 30% of the star surface. We argue that the X-ray emission is strongly enhanced due not only to the occurrence of these large scale magnetic structures, but also to their permanent interactions. These interactions lead to an uninterrupted flaring activity that generates large volume of hot plasmas. Since V390 Aurigae could be soon ascending the RGB, we anticipate that its rotation will spin-down dramatically with the effect of increasing its Rossby number and decreasing its helicity related dynamo driven activity. An hypothesis is that not only the rotational braking per se but also the restoration of rigid rotation could prevent the maintenance of large magnetic structures as the star ascends the red giant branch (Gondoin 1999). Rosner et al. (1995) pointed out that this suppression of a large scale dynamo leads to the disappearance of large scale organized stellar magnetic fields but does not imply the suppression of magnetic field production at small scale, driven by the turbulent motion in the surface convection zones. A bifurcation in magnetic loop sizes could occur as the dynamo induced by rotation gives way to a turbulent field generation mechanism like that described by Durney et al. (1993). According to this scenario, X-ray emission from large coronal loops and the related flaring activity should progressively disappear as V390 Aurigae evolves from G to K spectral type (see Fig. 6).

The above evolution scenario implies that, from the successive effects of convection zone deepening and rotational braking, a minimum value of the Rossby number is expected around V390 Aurigae's evolutionary stage. At this stage, $\alpha - \Omega$ dynamo mechanisms should operate with a maximum efficiency. Since hot coronal plasma conforms with the geometry of the magnetic field, the X-ray luminosity of V390 Aurigae should remain among the highest of the single giants. We compared our X-ray flux measurements of V390 Aurigae (see Sect. 4) in the 0.3 to 2 keV band with X-ray fluxes of single field giants extracted from the ROSAT all-sky survey catalogue (Hünsch et al. 1998). Upper limits of *Einstein* X-ray fluxes were also retrieved from Maggio et al. (1990). We calculated the X-ray luminosities ($L_X$) of all stars from the Hipparcos parallaxes. The results are presented in Fig. 6 as a function of $T_{\rm eff}$ for different mass ranges. The X-ray emission of giants reaches a maximum value in the effective temperature range $6000\ {\rm K} < T_{\rm eff} < 5000\ {\rm K}$ corresponding to G spectral types. Figure 6 confirms that the X-ray luminosity of V390 Aurigae is among the highest within this sample of single nearby F, G and K giants, thus supporting the above evolution scenario. The coronal structure and evolutionary status of V390 Aurigae would thus be similar to that of FK Comae (Gondoin et al. 2002). This justifies the classification of V390 Aurigae as an FK Comae-type star (Fekel & Marshall 1991). Both stars might be normal giants with A type progenitors on the main sequence that are evolving near the bottom of the red giant branch.

## 7. Summary

Our analysis of V390 Aurigae data suggests that the corona of this star is dominated by the same type of active region structure as on the Sun. However, the surface area coverage of these active regions approaches 30% and the size of the associated magnetic structures can be similar or larger than that of interconnecting loops between solar active regions while their temperature is hotter. The interaction of these structures most likely explains the permanent flaring activity on large scales that is responsible for heating V390 Aurigae plasma to coronal temperatures of $T \geq 10^7$ K. Based on V390 Aurigae position in the H–R diagram, we anticipate that its rotation will spin-down in the future with the effect of decreasing its helicity related, dynamo driven activity and suppressing large scale magnetic structures in its corona. The coronal structure and evolutionary status of V390 Aurigae is thus similar to that of FK Comae.

*Acknowledgements.* I thank my colleagues from the *XMM–Newton* Science Operation Center for their support in implementing the observations and Dr P. Papadopoulos for useful comments on the manuscript. I am grateful to the referee, Dr. J. Linsky, for the improvements brought to an earlier version of the manuscript.

## References

Allende Prieto, C., Lambert, D. L., & Asplund M. 2001, ApJ, 556, L63
Anders, E., & Grevesse, N. 1989, Geochim. Cosmochim. Acta, 53, 197
Antonucci, E., & Dodero, M. A. 1995, ApJ, 438, 480
Arnaud, K., & Dorman, B. 2001, XSPEC User's Guide for version 11.1, http://heasarc.gsfc.nasa.gov/docs/xanadu/xspec/manual/manual.html
Audard, M., Güdel, M., Drake, J. J., et al. 2000, ApJ, 541, 396
Audard, M., Güdel, M., & Mewe, R. 2001a, A&A, 365, L318
Audard, M., Behar, E., Güdel, M., et al. 2001b, A&A, 365, L329
Aschwanden, M. J., Nightingale, R. W., & Alexander, D. 2000, ApJ, 541, 1059
Bell, R. A., & Gustafsson, B. 1989, MNRAS, 236, 653
Bidelman, W. P. 1985, AJ, 90, 341
Brinkman, A. C., Gunsing, C. J. T., Kaastra, J. S., et al. 2000, ApJ, 530, 111
Brinkman, A. C., Behar, E., Güdel, M., et al. 2001, A&A, 365, L324
Collier Cameron, A. 1982, MNRAS, 200, 89
den Herder, J. W., Brinkman, A. C., Kahn, S. M., et al. 2001, A&A, 365, L7
de Medeiros, J. R., & Mayor, M. 1995, A&A, 302, 745
Dickey J. M., & Lockman F. J. 1990, ARA&A, 28, 215
Doschek, G. A., & Cowan, R. D. 1984, ApJS, 56, 67
Drake, J. J., Reale, F., Orlando, S., et al. 2000, ApJ, 545, 1074
Drake, N. A., Brickhouse, N. S., Kashyap, V., et al. 2001, ApJ, 548, L81
Drake, N. A., de la Reza, R., da Silva, L., et al. 2002, AJ, 123, 2703
Durney, B. R., & Latour, J. 1978, Geophys. Astrophys. Fluid Dyn., 9, 241
Durney, B. R., De Young, D. S., & Roxburgh, I. W. 1993, Sol. Phys., 145, 207
Ehle, M., Breitfellner, M., Dahlem, M., et al. 2001, The XMM–Newton Users' Handbook, http://xmm.vilspa.esa.es/user/AO2/uhb/xmm_uhb.html
Endal, A. S., & Sofia, S. 1979, ApJ, 232, 531
ESA 1997, The Hipparcos Catalogue, ESA SP-1200
Fekel, F. C., & Marschall, L. A. 1991, AJ, 102, 1439
Fekel, F. C., & Balachandran, S. 1993, ApJ, 403, 708
Gabriel, A. H., & Jordan, C. 1969, MNRAS, 145, 241
Gilliland, R. L. 1985, ApJ, 299, 286
Gondoin, P. 1999, A&A, 352, 217
Gondoin, P., Aschenbach, B., Erd, C., et al. 2000, SPIE Proc., 4140, 1
Gondoin, P., Erd, C., & Lumb., D. 2002, A&A, 383, 919
Gray, D. F. 1989, ApJ, 347, 1021
Gray, D. F., & Endal, A. S. 1982, ApJ, 254, 162
Griffiths, N. W., & Jordan, C. 1998, ApJ, 497, 1998
Güdel, M. 1997, ApJ, 480, L121
Güdel, M., Guinan, E. F., Mewe, R., et al. 1997a, ApJ, 479, 416
Güdel, M., Guinan, E. F., & Skinner, S. L. 1997b, ApJ, 483, 947
Güdel, M., Audard, M., Briggs, K., et al. 2001a, A&A, 365, L336
Güdel, M., Audard, M., Magee, H., et al. 2001b, A&A, 365, L344
Güdel, M., Audard, M., Kashyap, V. L., et al. 2003, ApJ, 582, 423
Gurzadyan, G. A. 1975, PASP, 87, 289
Hooten, J. T., & Hall, D. S. 1991, ApJS, 74, 225
Huenemoerder, D. P., Canizares, C. R., & Schulz, N. S. 2001, ApJ, 559, 1135
Hünsch, M., Schmitt, J. H. M. M., & Voges, W. 1998, A&AS, 127, 251
Jansen, F., Lumb, D., Altieri, B., et al. 2001, A&A, 365, L1
Kashyap, V. L., Drake, J. J., Güdel, M., et al. 2002, ApJ, 580, 1118
Kholopov, P. N., Samus, N. N., Kazarovets, E. V., et al. 1989, Inf. Bull. Variable Stars, No. 3323
Konstantinova-Antova, R. K., Antov, A. P., & Bachev, R. S. 2000, Inf. Bull. Variable Stars, No. 4867
Kucera, T. A., Dennis, B. R., Schwartz, R. A., et al. 1997, ApJ, 475, 738
Lemen, J. R., Mewe, R., Schrijver, C. J., et al. 1989, ApJ, 341, 474
Lemoine, M., Vidal-Madiar, A., Hebrard, G., et al. 2002, ApJS, 140, 67
Leonard, P. J. T., & Livio, M. 1995, ApJ, 447, L121
Liedahl, D. A., Osterheld, A. L., & Goldstein, W. H. 1995, ApJ, 438, 115
Maggio, A., Vaiana, G. S., Haisch, B. M., et al. 1990, ApJ, 348, 253
Mewe, R., Gronenschild, E. H. B. M., Heise, J., et al. 1982, ApJ, 260, 233
Mewe, R., Gronenschild, E. H. B., & van den Oord, G. H. J. 1985, A&A, 62, 197
Mewe, R., Kaastra, J. S., White, S. M., et al. 1996, A&A, 315, 170
Mewe, R., Raassen, A. J. J., Drake, J. J., et al. 2001, A&A, 368, 888
Murphy, R. J., Ramaty, R., Reames, D. V., et al. 1991, ApJ, 371, 793
Ness, J. U., Mewe, R., Schmitt, J. H. M. M., et al. 2001, A&A, 367, 282
Ness, J. U. R., Schmitt, J. H. M. M., Burwitz, V., et al. 2002, A&A, 394, 911
Osten, R. A., Ayres, T. R., Brown, A., et al. 2003, ApJ, 582, 1073
Pradhan, A. K. 1982, ApJ, 263, 477
Reale, F., Peres, G., & Orlando, S. 2001, ApJ, 557, 906
Rosner, R., Tucker, W. H., & Vaiana, G. S. 1978, ApJ, 220, 643
Rosner, R., Musielak, Z. E., Cattaneo, F., et al. 1995, ApJ, 442, L25
Rutten, R. G. M., & Pylyser, E. 1988, A&A, 191, 227
Sanz-Forcada, J., Brickhouse, N. S., & Dupree, A. K. 2002, ApJ, 570, 799
SAS 2001, XMM–Newton Science Analysis System, Reference Documentation, http://xmm.vilspa.esa.es/user/sas_top.html
Schaller, G., Schaerer, D., Meynet, G., et al. 1992, A&AS, 96, 269
Schmelz, J. T. 1993, ApJ, 408, 373
Schmitt, J. H. M. M., Collura, A., Sciortino, S., et al. 1990, ApJ, 365, 704
Schmitt, J. H. M. M., Drake, J. J., & Stern, R. A. 1996, ApJ, L465, 51
Schmitt, J. H. M. M., & Ness, J. U. 2002, A&A, 388, L13
Schrijver, C. J., van den Oord, G. H. J., Mewe, R., et al. 1995, A&A, 302, 438
Sills, A., Lombardi, J. C., Bailyn, C. D., et al. 1997, ApJ, 487, 290
Simon, T., & Drake, S. A. 1989, ApJ, 346, 303
Spurr, A. J., & Hoff, D. 1987, Inf. Bull. Variable Stars, No. 3028
Strassmeier, K. G., Kekel, F. C., Bopp, B. W., et al. 1990, ApJS, 192, 71
Strüder, L., Briel, U., Dennerl, K., et al. 2001, A&A, 365, L18
Tsuru, T., Makishima, K., Ohashi, T., et al. 1989, PASJ, 41, 679
Turner, M. J. L. T., Abbey, A., Arnaud, M., et al. 2001, A&A, 365, L27
Vaiana, G. S., Davis, J. M., Giacconi, R., et al. 1973, ApJ, 185, 47
Vaiana, G. S., & Rosner, R. 1978, ARA&A, 16, 393
van den Oordt, G. H. J., & Mewe, R. 1989, A&A, 213, 245
van Speybroeck, L. P., Krieger, A. S., & Vaiana, G. S. 1970, Nature, 227, 818